

Scaling laws of band gaps of phosphorene nanoribbons: a tight-binding calculation

Esmail Taghizadeh, Mohammad H. Zare, and Farhad Fazileh

Department of Physics, Isfahan University of Technology, Isfahan 84156-83111, Iran

(Dated: June 5, 2022)

We study the band structure and electronic transport of monolayer black phosphorus (phosphorene) zigzag and armchair nanoribbons, which are modeled by a five parameter tight-binding approximation. In zigzag nanoribbons, we found that the ratio of the two dominant hopping parameters specifies whether a pair of separate quasi-flat bands at the Fermi level would exist. We found that the corresponding states are edge localized if their bands are well separated from the valence and conduction bands. Also, we investigated the scaling laws of the band gaps versus ribbon widths for armchair and zigzag phosphorene nanoribbons. We found that for armchair nanoribbons the scaling law is $\sim 1/w^{1.92}$, and for zigzag nanoribbon it is $\sim 1/w^{1.65}$. In armchair nanoribbons the transverse electric field along the ribbon width closes the band gap by shifting the energy of the valence and conduction band edge states. For small widths, we found that further increase in the field opens the gap again, which is connected to the finite effective interactions between opposite edge states. The closure of the band gap for larger strengths of the field is discussed to be connected to the special structure of this system. For zigzag nanoribbons a gap is opened at the relatively degenerate quasi-flat bands which makes these ribbons a promising candidate for the future of field effect transistors.

I. INTRODUCTION

Two-dimensional structures inspired by graphene such as hexagonal Boron Nitride (BN) and transition metal dichalcogenides (TMDs) have attracted considerable attentions due to their remarkable electronic properties¹⁻⁸. Graphene is known to have novel electronic and mechanical properties such as high carrier mobility, but its zero band gap limits its performance. Molybdenum disulfide (MoS₂) as a TMD possesses a direct band gap of ~ 1.8 eV⁹ and relatively high on/off ratio¹⁰. However the carrier mobility of MoS₂ is much less than graphene. These layered structures can be etched or patterned to quasi-one-dimensional strips, called nanoribbons. Graphene nanoribbons (GNRs) and MoS₂ nanoribbons are examples of these 1D strips. These one-dimensional nanoribbons etched or patterned from above mentioned 2D materials can offer even more tunability in electronic structures due to the quantum confinement and edge effects¹¹⁻¹³.

Recently, monolayer black phosphorus, called "phosphorene", has attracted much attention due to its potential applications in nano-electronics, thermo-electronics and opto-electronics¹⁴⁻¹⁸. Phosphorene has a finite band gap and a larger mobility comparing to MoS₂. Similar to bulk graphite, black phosphorus is also a layered structure that the layers are stacked together by van der Waals interactions¹⁹. Each layer consists of phosphorus atoms covalently bonded with three adjacent phosphorus atoms making a puckered honeycomb structure due to sp^3 hybridization as depicted in Fig. 1. It is shown in this figure that phosphorus sites are grouped in two zigzag layers, where upper sites are shown with darker color, whereas the lower ones are shown with lighter colors. Phosphorene has been successfully obtained by several groups in the laboratory¹⁴⁻¹⁸. Similar to graphene, that is isolated by peeling, phosphorene can also be isolated from black

phosphorus by mechanical exfoliation. Phosphorus has a direct band gap of 0.3 eV^{15,20-22}. By mechanically exfoliating from bulk phosphorus, few layers of phosphorene can be obtained, which has a band gap, depending on the thickness, ranging from 1.5 eV for monolayer to 0.6 eV for five-layers²³. Although phosphorene nanoribbons (PNRs) have yet to be fabricated, experience from graphene and other 2D materials suggests that any predictions of the electronic structure and optical properties of PNRs are essential for the the future research of phosphorene-based nanoelectronics.

There are already many works based on first-principle calculations²⁴⁻²⁷. Recently, a tight-binding model has been proposed by introducing hopping integrals t_i over 5 neighbouring sites²⁸ as illustrated in Fig. 1.

Our goal is to apply the above mentioned tight-binding model for phosphorene zigzag and armchair nanoribbons and calculate the band structure and quantum conductance of the ribbons and compare the results with other more sophisticated calculations. Then, we examine the effect of the application of transverse electric field on the band structure and quantum conductance of both zigzag and armchair nanoribbons.

In the next section the model is introduced in details, then in section III the numerical data for this model is presented. The emergence of edge states and the gradual emergence of flat bands in zigzag nanoribbons by increasing the $|t_2/t_1|$ ratio is discussed. The power law scaling of band gap versus the ribbon width is provided and is compared with other methods. This section is followed by the numerical data for the effect of a transverse electric field and the discussion on the transistor effect in zigzag ribbons.

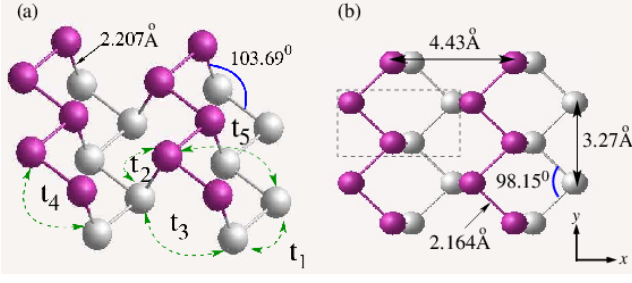


FIG. 1. (a) Crystal structure and hopping integrals t_i of a single layer phosphorene for the tight-binding model. (b) Top view. The dark (grey) balls represent phosphorus atoms in the upper (lower) layer. The dotted rectangle represents a primitive unit cell containing four atoms. The parameters for the bond angles and unit cell lengths are taken from¹⁷.

II. MODEL HAMILTONIAN

The tight-binding Hamiltonian recently proposed for this system²⁸ is given by

$$H = \sum_{\langle i,j \rangle} t_{ij} c_i^\dagger c_j \quad (1)$$

where summation is over the lattice sites, and t_{ij} are the hopping integrals between i th and j th sites, and c_i^\dagger and c_j represent the creation and annihilation operators of electrons on sites i and j , respectively. These hopping integrals between a site and its neighbours are shown in Fig. 1.

The connections in each zigzag chain in the upper or lower layer are representing the t_1 hoppings, and the connections between a pair of upper and lower zigzag chains represent the t_2 hopping integrals. t_3 is between the nearest sites of a pair of zigzag chains in the upper or lower layer, and t_4 is the hopping between the next nearest neighbour sites of a pair of the upper and lower zigzag chains. t_5 is the hopping between two atoms on upper and lower zigzag chains that are farthest from each other. The explicit values of these hoppings as suggested by²⁸ reads $t_1 = -1.220\text{eV}$, $t_2 = 3.665\text{eV}$, $t_3 = -0.205\text{eV}$, $t_4 = -0.105\text{eV}$, and $t_5 = -0.055\text{eV}$. The special character of this model is that the second hopping integral is positive. This implies zigzag chains with negative t_1 hoppings along the chains and positive t_2 hoppings that connect these chains. For zigzag nanoribbons, the eigenstates of the transverse modes, which characterize the behaviour of the states as edge states or bulk states are along both t_1 and t_2 connections. As depicted in Fig. 1 the unit cell of phosphorene is a rectangle containing four phosphorus atoms.

III. NUMERICAL RESULTS AND ANALYSIS

In order to understand the physics of this model, we study the role of each hopping parameter played in the

behaviour of the electronic structure of this model for both zigzag phosphorene nanoribbons (zPNRs) and arm-chair phosphorene nanoribbons (aPNRs). We are using the usual convention that is used for identifying the width size of graphene nanoribbons¹¹ to identify the PNR structures. In accordance with this convention, the aPNR structure is defined by the number of dimmer lines in the width of the ribbon (N_a -aPNRs) and the zPNR is defined by the number of zigzag chains in the width of the ribbon (N_z -zPNRs)²⁹. For calculation of the band structure and eigenstates of the nanoribbons, we obtain the eigenvalues and eigenvectors of the following matrix,

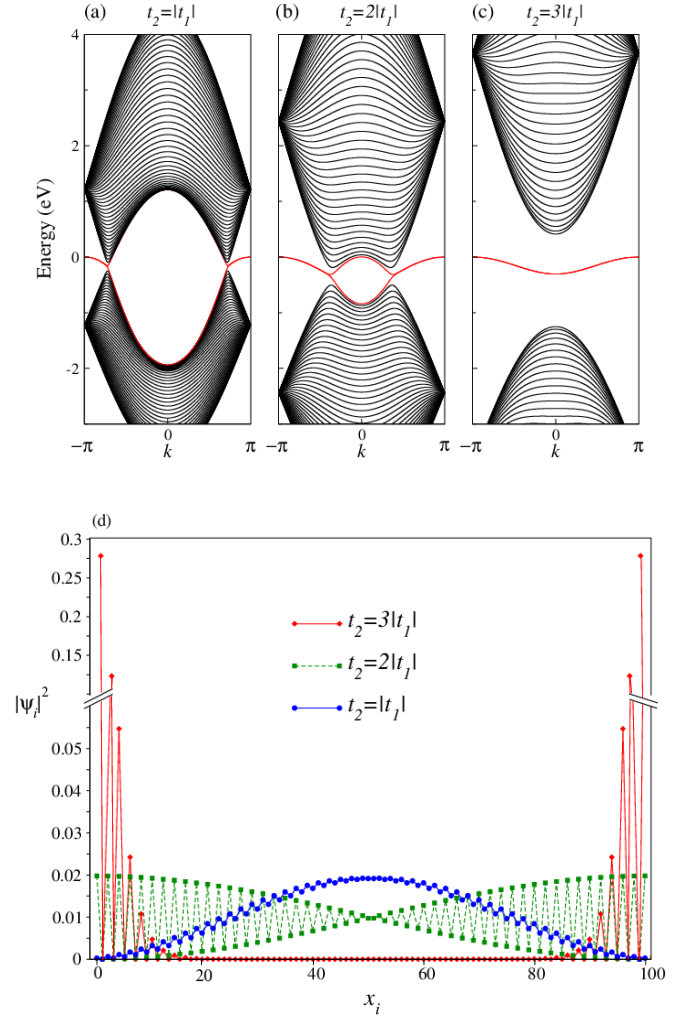


FIG. 2. Top: The band structure of 100-zPNRs along $\Gamma - X$ direction for different values of the $|t_2/t_1|$ ratio, (a) $|t_2/t_1|=1$, (b) $|t_2/t_1|=2$, and (c) $|t_2/t_1|=3$, while $t_3 = -0.205$, $t_4 = -0.105$, and $t_5 = -0.055$. The red lines show the edge bands. Bottom: The probability amplitude of the VBM eigenstate of a zigzag phosphorene nanoribbon for different ratios of $|t_2/t_1|$ for $k_x = 0$. The horizontal axis is the site labeling of a unit cell in the width of the ribbon.

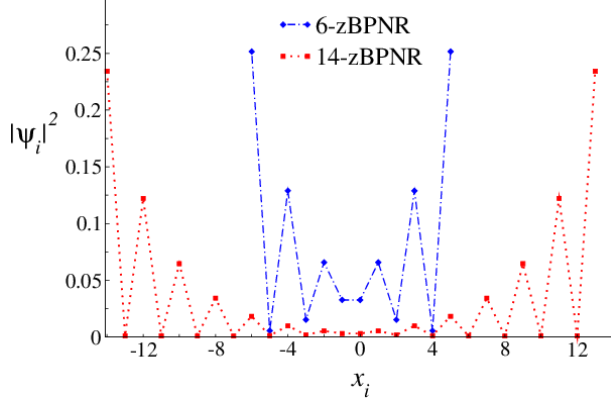


FIG. 3. The probability amplitude of the VBM eigenstates of zPNRs for different widths of 6-zPNRs and 14-zPNRs. The horizontal axis is the site labeling of a unit cell in the width of the ribbon.

which is the crystal Hamiltonian between the Bloch sums

$$M_{\alpha\beta}(\mathbf{k}) = - \sum_{ij} t_{i\alpha;j\beta} e^{i\mathbf{k} \cdot \mathbf{R}_{ij}} \quad (2)$$

where i and j label different unit cells, α and β label basis sites in a unit cell, \mathbf{k} is the wave vector, \mathbf{R}_{ij} represents a bravais lattice vector, and $t_{i\alpha;j\beta}$ is the hopping integral between basis site α of unit cell i and basis site β of unit cell j and they will be substituted by the five hopping parameters of the model accordingly. For nanoribbons the periodicity is only along the ribbon length and therefore the number of basis sites in each unit cell is proportional to the ribbon width.

A. Edge modes in zPNRs

We start with studying the dependence of the behaviour of the flat bands and their corresponding edge states in the zPNRs on the ratio of $|t_2/t_1|$. The band structure and the probability amplitude of the valence band eigenstates of zPNRs for three values of this ratio, $|t_2/t_1| = 1, 2$, and 3 , for 100-zPNRs are shown in Fig. 2. As can be seen in Fig. 2(a), (b) and (c), by increasing the $|t_2/t_1|$ ratio the two middle bands, which are shown by red lines in the figure, are detached from the bulk bands. The critical value of the ratio for emergence of the edge states at $k = 0$ is 2 , i.e. for this ratio the average amplitude of $|\Psi_i|^2$ becomes almost homogeneous in the bulk. It should be noted that the states corresponding to the quasi-flat bands outside the middle region, e.g. between the Dirac like points and $k = \pi$ or $k = -\pi$ are always localized on the edges. Fig. 2(c) shows the band structure for $|t_2/t_1| = 3$. In this case, the edge bands are isolated from the bulk states and they are two-fold degenerate. This degeneracy is lifted in zPNRs

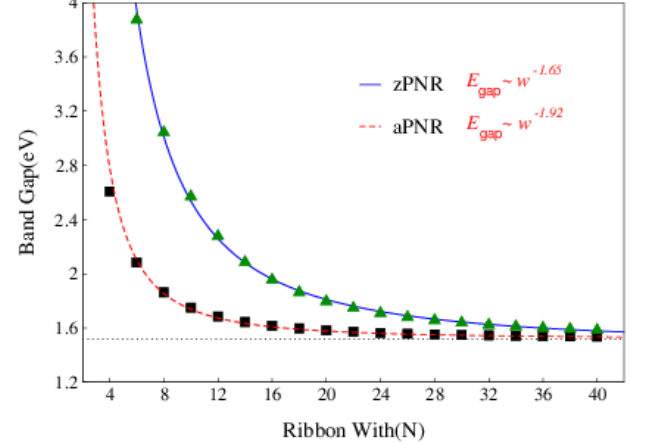


FIG. 4. The scaling law of the band gap of zPNRs and aPNRs versus the ribbon width.

with small widths ($N_z < 40$) for the wavevectors around $k_x = 0$. This behaviour can be simply explained by taking into account the effect of the finite electron tunneling between two opposite edges for the small width zPNRs³⁰. In Fig. 2(d), you can find the probability amplitude of the valence band maximum (VBM) as a function of the position of the phosphorus atoms. It is obvious that for the small values of this ratio, the probability amplitude for the bulk sites is large, while for the edge sites it is very small or even zero. By increasing this ratio, the probability amplitude of the bulk sites begin to decrease. For the $|t_2/t_1| = 3$, only the probability amplitude of the sites near the edges are non-zero and this shows the important role of the $|t_2/t_1|$ ratio in the creation of the edge states. If we set $t_4 = 0$, the edge bands become perfectly flat.

The other factor for the creation of the edge states in zPNRs is the ribbon width. The ribbon width in zPNRs needs to be larger than a minimum limit for the edge states to be able to appear. Fig. 3 shows the squared wave functions of the VBM states of 6-zPNRs and 14-zPNRs. By increasing the ribbon width, these states become localized on the phosphorus atoms close the two edges. The minimum width for the creation of the edge bands in zPNRs is about 3 nm which is related to the 14-zPNR. For the zPNRs with widths larger than 3 nm, the wave function related to the two edges start to decouple and it will localize on opposite edges. It should be noted that according to this tight-binding model the edge bands do not exist in armchair PNRs (aPNRs), however there are other works based on first-principle calculations that predict edge bands even for aPNRs³¹.

B. Scaling laws of band gaps for PNRs

Fig. 4 shows the dependence of the band gap attributed to the ribbon width for zPNRs and aPNRs. This de-

pendence to the ribbon width arises from the quantum confinement effects^{32–35}. Based on DFT calculations the scaling behavior of the band gap with increasing the ribbon width for both types of PNRs has been calculated^{29,36}. The scaling behavior of the band gap for aPNRs is $\sim 1/w^2$ but for zPNRs is $\sim 1/w$. It should be noted that the DFT-calculated band gap for phosphorene is about 1eV that is very different from the experimental value which is about 1.45eV¹⁵ whereas the band gap from the calculations based on GW approach is about 1.5eV^{28,37}. As is depicted in Fig. 4, based on our tight-binding model the scaling law of the band gap for aPNRs is $\sim 1/w^{1.92}$ and for zPNRs is $\sim 1/w^{1.65}$. The origin of the different behavior in the scaling law of the band gap for the two PNRs is rooted in the difference in the curvature of energy-momentum dispersion along Γ -X and Γ -Y directions²⁹. Based on our calculations for PNRs with large width, the band gap for the aPNRs converges to 1.52eV whereas for the zPNRs it converges to 1.48eV. These results are in good agreement with the experimental value and the results of the GW approach. In contrast to the boron nitride nanoribbons (BNNRs)³⁸, graphene nanoribbons (GNRs)³² and α -graphdiyne nanoribbons (α -GNRs)³⁹, the band gap of the PNRs monotonically decreases with the increase of the ribbon width. By increasing the ribbon width, the band gap in aPNRs drops much faster than the zPNRs. This implies that the quantum confinement effect in aPNRs is stronger than that in zPNRs.

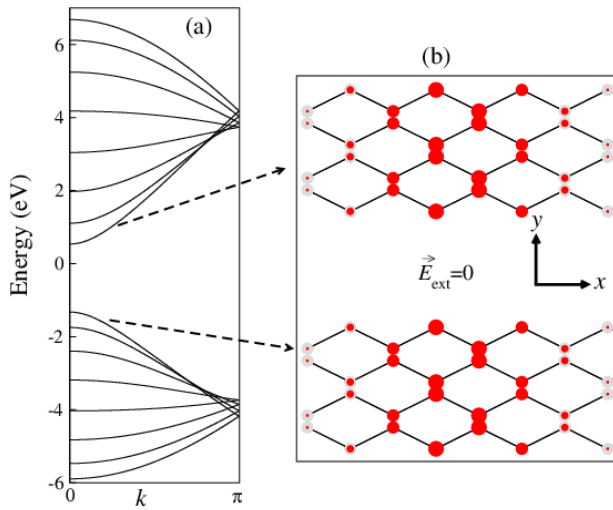


FIG. 5. (a) band structure and (b) probability amplitudes of the armchair phosphorene nanoribbon for zero transverse electric field. The eigenstates are related to the $k = 0$ point of the brillouin zone.

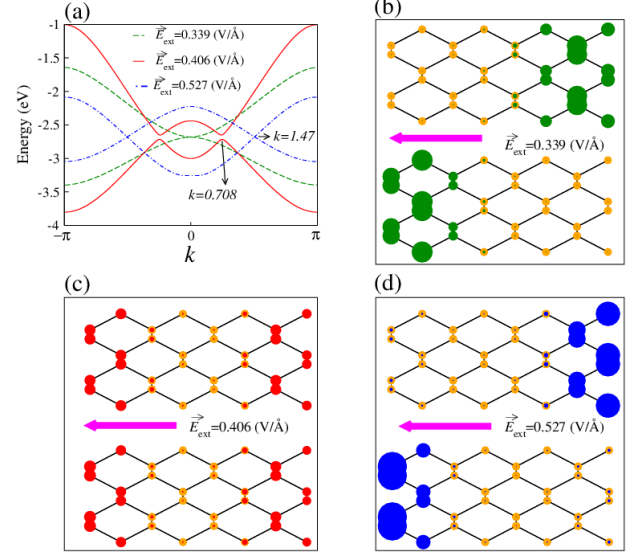


FIG. 6. (a) Conduction and valence bands (CB and VB) of a 8-aPNR under a transverse electric field for three values of $E_{ext} = 0.339, 0.406, 0.527$ V/Å. (b), (c), and (d) Amplitudes of the eigenstates of the CB and VB for these three values of external electric field.

C. Response of aPNRs to E_{ext}

In the next step we study the dependence of the electronic properties of the aPNRs (the periodicity is along the y-direction) to the external electric field, E_{ext} . From the band structure (shown in Fig. 5(a)) for $E_{ext} = 0$, it is clear that the size of the band gap for the ribbon is determined by the position of the conductance band (CB) and valence band (VB). The electronic states associated with the VB and CB states are located in the

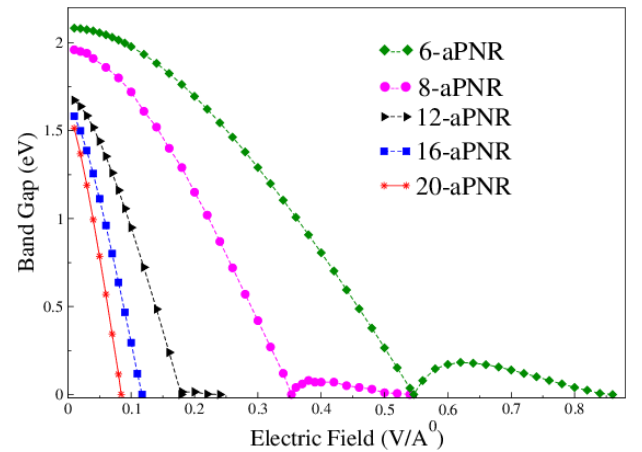


FIG. 7. Variation of the band gap of aPNRs versus transverse external electric field for five different ribbon widths.

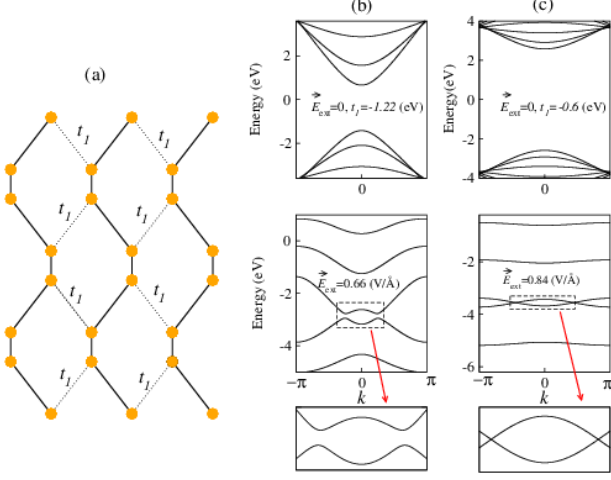


FIG. 8. Effect of t_1 on the opening of the band gap for small width aPNRs with an applied transverse electric field. (a) schematic of the sample ribbon. (b) band structure without any external field and for $E_{ext} = 0.66 \text{ V/Å}$ for $t_1 = 1.22 \text{ eV}$. (c) The same as (b) but for $E_{ext} = 0.84 \text{ V/Å}$ and $t_1 = 0.6 \text{ eV}$.

bulk of the ribbon (Shown in Fig. 5(b)). Since the Fermi energy is located in the band gap, all aPNRs are semiconductors independent of their ribbon width. When the transverse E_{ext} is applied, due to Stark effect the states corresponding to the CB which have a positive band curvature (electron states) will shift to lower energies while the states corresponding to VB (hole states) shift to higher energies. This means that the CB and VB states will localize on ribbon edges. By increasing the field even further due to the electrostatic potential difference between the opposite edges the two bands approach together and the band gap is decreasing and eventually it is closing at $E_{ext} = 0.339 \text{ V/Å}$ (Fig. 6(a)). The edge states of this configuration at $k = 0$ for the VB and CB are depicted in Fig. 6(b). By increasing the external transverse electric field the band gap opens again. As is depicted in Fig. 6(a) for $E_{ext} = 0.406 \text{ V/Å}$ the VBM and CBM shifts to $k = 0.72$, and there is a finite band gap at this point. The eigenstates at this point have amplitudes at both edges as depicted in Fig. 6(c). Again for $E_{ext} = 0.527 \text{ V/Å}$ the band gap closes, but this time at $k = 1.47$ and the dispersion is linear at these points, which is something similar to Dirac points in graphene. The eigenstates at these points are localized at edges as shown in Fig. 6(d).

For the critical transverse field, E_c , where the band gap closes, e.g. the insulator-metal transition point, the wave functions of the highest occupied state (HOS) and the lowest empty state (LES) are localized on the two opposite edges. Such a behavior for the band gap variation as function of the E_{ext} have been already observed in other materials such as, GNRs³², carbon nanotubes⁴⁰, MoS₂³⁰ and BN nanoribbons (BNNRs)^{35,38,41}. It is worth noting

that in contrast to other compounds such as BN³⁸, the gap closure is independent of the direction of the transverse E_{ext} .

We also calculated the change of the band gap of aPNRs as a function of the E_{ext} for four different widths (Shown in Fig. 7). As the transverse E_{ext} increases, the band gap uniformly decreases. Similar behaviors have also been observed in the nanoribbons of BN^{35,38} and MoS₂³⁰. By increasing the aPNR width the band gap decreases much faster as the transverse field increases and the critical field, E_c , for closing the gap reduces. This is due to the fact that the electrostatic potential difference is proportional to the ribbon width. Recently, DFT-calculated results have obtained the width dependent of the band gap modulation induced by the transverse E_{ext} ³⁶. For aPNRs with large widths, our results based on the tight-binding approach are in a good agreement with the DFT-calculated results. By increasing the transverse E_{ext} , the gap is directly closed in Γ point and the edge band states related to the VBM and CBM states are completely localized on the opposite edges of the aPNRs. For the aPNRs with the different widths, the insulator-metal transition occurs for the various values of E_c . As is shown in Fig. 7, an intriguing behavior exists in the gap closure of the aPNRs with the small widths. Such as for the 8-aPNR, the band gap changes slowly in the large E_{ext} and also the band gap is closed for two values of $E_c = 0.339$ and 0.527 . Fig. 6a shows the HOS and LES for three different values of $E_{ext} = 0.339, 0.406$ and 0.527 . For $E_c = 0.339$, the band gap is directly closed in the Γ point and the wave functions associated with VBM and CBM are completely localized on the opposite edges (Shown in Fig. 6b). By increasing the E_{ext} , the gap again opens and the position of the band gap shifts away from the Γ point. The HOS and LES wave functions attributed to $E_{ext} = 0.406$ are shown in Fig. 6c. In this case, the HOS and LES wave functions have non-zero values on both edges. Then due to the hopping integral between the two edges, the degeneracy is lifted³⁰. In the following discussion we would explain this issue in more details. For $E_{ext} = 0.527$, the band gap again is closed and the insulator-metal transition occurs and also the HOS and LES wave functions are again localized in the opposite edges (Shown in Fig. 6d).

Here we aim to explain what factors are important in opening the band gap after it is closed by increasing the transverse electric field for the smaller width aPNRs. As we discussed, for 8-aPNRs at $E_{ext} = 0.406$ the wave functions of the HOS and LES are localized on both edges. The small width allows the electrons from both edges to jump to the opposite edge with a finite probability. This interaction will lift the degeneracy which is created by crossing the CB and VB when the E_{ext} is increased, and it opens up a gap which should be almost constant if we model the edge states with two linear chains that are connected with an small effective hopping integral. This behavior has been explained in³⁰ and it is discussed that the closure of the gap in the end is related to the

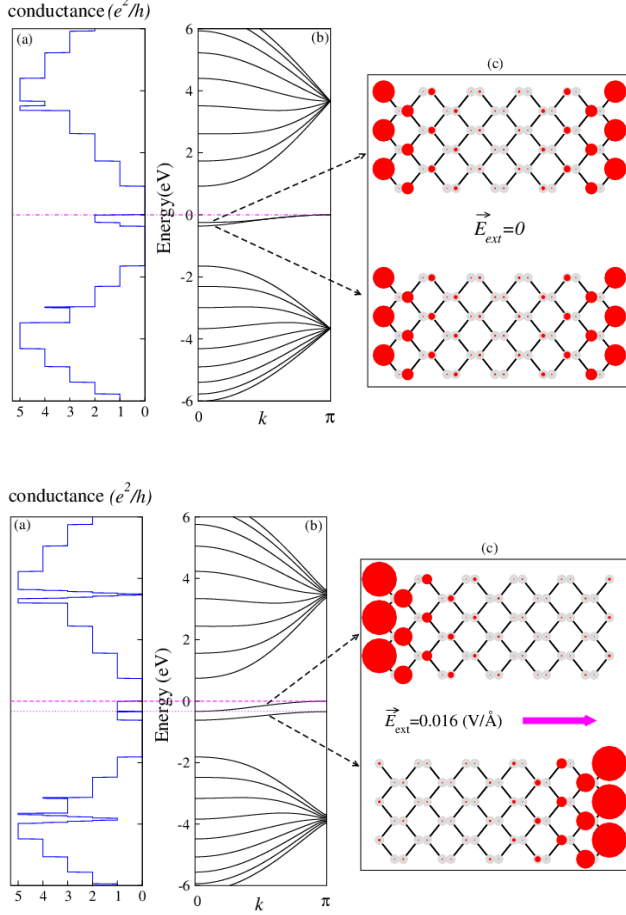


FIG. 9. Top: (a) Conductance, (b) band structure, and (c) probability amplitudes of the band gap edge states of a zPNR for zero transverse electric field. Bottom: The same graph but for $E_{ext} = 0.016$ V/Å. The eigenstates are related to the Γ point of the Brillouin zone.

polarization of the structure and the modification of the atomic bonds in the ribbon edges. Here in our model the situation is much simpler and we are not considering any polarization while the band is closing at two points. This behavior suggests that the closure of the band gap here is dominantly controlled by the special structure of this system and not by polarization. In Fig. 8, we have investigated the effects of the different hopping integrals on opening the band gap for a 6-aPNR. As is shown in Fig. 8a, the electrons can transfer between the opposite edges by the hopping integrals of t_1 , t_3 , t_4 and t_5 . We found that by setting $t_3, t_4, t_5 = 0$ the general trends of the band structure does not change and so the role of the t_1 is dominant in opening of the gap. Figs. 8b and 8c show the changes of the band gap with respect to the different values of t_1 . For $t_1 = -1.22$ eV, a gap is opened between the HOS and LES (Shown in Fig. 8b). As we decrease the value of t_1 to 0.7, the band gap is closed (Shown in Fig. 8c). As a consequence, the interaction

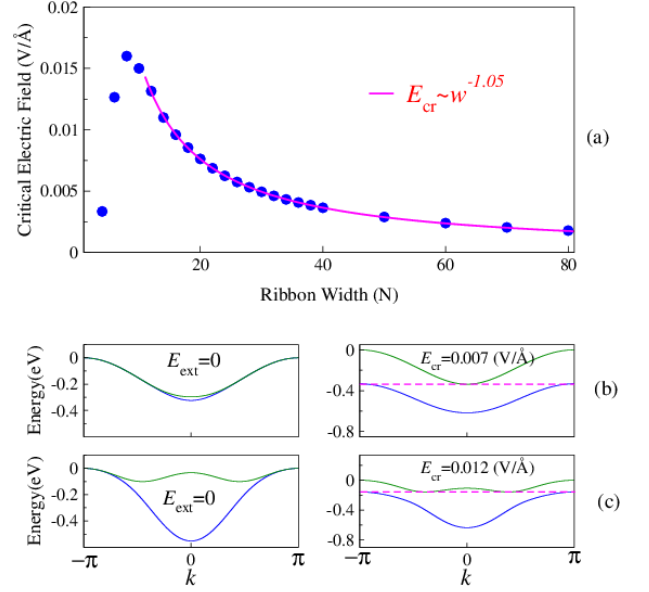


FIG. 10. (a) Scaling of the critical transverse electric field for the vanishing of the overlap of the quasi-flat bands in terms of ribbon width. (b) Quasi-flat bands for a 8-zPNR for $E_{ext} = 0$ and $E_{ext} = E_c$. (c) Same as (b) but for a 14-zPNR.

between the ribbon's edges increases when the ribbon width reduces. Then for the aPNRs with the small widths, a strong band repulsion is formed at the band gap. A similar behavior has been already observed in MoS₂³⁰.

D. Transistor effect in zPNRs

Recently a work based on tight-binding model have studied the effect of the external in-plane (E_x) electric field on the edge modes of zPNRs and also the effect of the external electric field (E_z) perpendicular to the ribbon surface for zPNRs⁴². The results show that the band gap increases according to $(lE_z)^2$ where l is the separation distance between the upper and lower layers of phosphorene. Also, for E_x larger than a critical strength (E_c), the degeneracy of the edge bands in Fig. 2c for the quasi-flat bands is lifted and a transistor effect is observed. The E_c is inversely proportional to the ribbon width ($\propto 1/w$).

In this work, we investigated the transistor effect in zPNRs in more details by using the Landauer formalism^{43,44}. In this formalism, the conductance $\sigma(E)$ for nanoscale devices at Fermi energy (E) between a pair of leads p and q is given by:

$$\sigma(E) = \left(\frac{e^2}{h}\right) Tr[\Gamma_p(E)G_D^R(E)\Gamma_q(E)G_D^A(E)] \quad (3)$$

where $G_D^R(E)$ is the Green function of the sample and $G_D^A(E) = G_D^R(E)^\dagger$. In this equation, $\Gamma_{p(q)} = i[\Sigma_{p(q)}(E) - \Sigma_{p(q)}^\dagger(E)]$ where $\Sigma_{p(q)}(E)$ is the self energy related to lead p (q). The Green's function of the device ($G_D^A(E)$) is given by

$$G_D^A(E) = [E - H_D - \Sigma_p(E) - \Sigma_q(E)]^{-1} \quad (4)$$

We proceed our discussions when the transistor effect can be observed in zPNRs. The conductance, band structure and wave functions of a 8-zPNRs for $E_{ext}=0$ and 0.016 are shown in Fig. 9. It is shown in Fig. 9b that the degeneracy between the two edge modes at zPNRs is slightly lifted close to $k_x = 0$. The conductance is therefore slightly asymmetric around $k_x = 0$. As is shown in Fig. 9c the wave functions of upper and lower quasi-flat bands are localized on both edges. By increasing the external electric field at a critical field the overlap between these two bands vanishes and we find a conductance controlled by external electric field at Fermi energy, a field effect transistor behavior. In this case, the wave functions of upper and lower edge bands are localized on the opposite edges (Shown in Fig. 9f).

In the following we considered the behavior of E_c as a function of the ribbon width (Shown in Fig. 10a). For zPNRs with widths larger than $N_z = 14$, E_c scales like $1/w^{1.05}$ which is in good agreement with the previous results by Ezawa⁴². But for the ribbons with widths smaller than $N_z = 14$, we found a completely different behavior. To explain this region of the graph we considered the behavior of the edge bands for zPNRs with the different widths. Fig. 10b shows the quasi-flat bands for 14-zPNR, while Fig. 10c shows it for 8-zPNR. For $E_{ext} = 0$, the quasi-flat bands for these two widths are

different. The VBM and CBM of 14-zPNR are located at $k_x = \pi$ and $k_x = 0$, respectively. The VBM of 8-zPNR is also located at $k_x = \pi$, while the CBM of 8-zPNR is located at a k_x between 0 and π . This displacement of the CBM in 8-zPNR is caused by the finite interaction between the two edge modes. This displacement of the CBM in zPNR with small widths, which is originated from the finite interaction between the opposite edge modes, provides the advantage of a lower external electric field needed for observation of the transistor effect.

IV. CONCLUSION

In summary, our numerical results based on a five parameter tight-binding model for PNRs show that zP- NRs are always metal and aPNR are semiconductors independent of the their ribbon width. Our method for the zP- NRs predict a pair of degenerate quasi-flat bands at the Fermi level that are localized on the ribbon edges and this degeneracy is lifted for small ribbon widths due to finite interactions between the edge states. Also our calculations reveal scaling laws of the band gap for PNRs versus the ribbon width which for aPNRs it is $\sim 1/w^{1.92}$, while for zPNRs it is $\sim 1/w^{1.65}$. An external transverse electric field can remove the overlap between these flat bands and this behavior, a device with field dependent conductance, is a promising candidate for the future of field effect transistors. For the aPNRs we predict a semiconducting behavior that by applying a transverse electric field we expect an insulator-metal transition. Our results based on the relatively simple tight-binding model are in good agreement with ab initio calculations and this suggests that this model can provide a reasonable basis for studying the electronic properties of this system.

- ¹ K. S. Novoselov, A. K. Geim, S. V. Morozov, D. Jiang, Y. Zhang, S. V. Dubonos, I. V. Grigorieva, and A. A. Firsov, *Science* **306**, 666 (2004).
- ² A. K. Geim and K. S. Novoselov, *Nature Materials* **6**, 183 (2007).
- ³ A. H. C. Neto, F. Guinea, N. M. R. Peres, K. S. Novoselov, and A. K. Geim, *Rev. Mod. Phys.* **81**, 109 (2009).
- ⁴ A. Splendiani, L. Sun, Y. Zhang, T. Li, J. Kim, C. Y. Chim, G. Galli, and F. Wang, *Nano Lett* **10**, 1271 (2010).
- ⁵ K. F. Mak, C. Lee, J. Hone, J. Shan, and T. F. Heinz, *Phys. Rev. Lett* **105**, 136805 (2010).
- ⁶ D. Xiao, G. B. Liu, W. Feng, X. Xu, and W. Yao, *Phys. Rev. Lett* **108**, 196802 (2010).
- ⁷ X. Blase, A. Rubio, S. G. Louie, and M. L. Cohen, *Phys. Rev. B* **51**, 6868 (1995).
- ⁸ K. Watanabe, T. Taniguchi, and H. Kanda, *Nature Materials* **3**, 404 (2004).
- ⁹ A. Kuc, N. Zibouche, and T. Heine, *Phys. Rev. B* **83**, 245213 (2011).

- ¹⁰ B. Radisavljevic, A. Radenovic, J. Brivio, V. Giacometti, and A. Kis, *Nature Nanotechnology* **6**, 147 (2011).
- ¹¹ Y. W. Son, M. L. Cohen, and S. G. Louie, *Nature (London)* **444**, 347 (2006).
- ¹² L. Yang, M. L. Cohen, and S. G. Louie, *Nano Letters* **7**, 3112 (2007).
- ¹³ X. Wang, Y. Ouyang, X. Li, H. Wang, J. Guo, and H. Dai, *Phys. Rev. Lett* **100**, 206803 (2008).
- ¹⁴ L. Li, Y. Yu, G. J. Ye, Q. Ge, X. Ou, H. Wu, D. Feng, X. H. Chen, and Y. Zhang, *Nature Nanotechnology* **9**, 372 (2014).
- ¹⁵ H. Liu, A. T. Neal, Z. Zhu, X. Xu, D. Tomanek, and P. D. Ye, *ACS Nano* **8**, 4033 (2014).
- ¹⁶ F. Xia, H. Wang, and Y. Jia, *Nature Communications* **5**, 4458 (2014).
- ¹⁷ A. Castellanos-Gomez and et. al., *2D Materials* **1**, 025001 (2014).
- ¹⁸ S. P. Koenig, R. A. Doganov, H. Schmidt, A. H. C. Neto, and B. Oezylmaz, *Appl. Phys. Lett.* **104**, 103106 (2014).
- ¹⁹ A. Morita, *Appl. Phys. A* **39**, 227 (1986).

- ²⁰ D. Warschauer, J. Appl. Phys. **34**, 1853 (1963).
- ²¹ S. Narita, Y. Akahama, Y. Tsukiyama, K. Muroa, S. Morita, S. Endo, M. Taniguchi, M. Seki, S. Suga, A. Mikuni, and et. al., Physica **117B**, 422 (1983).
- ²² Y. Maruyama, S. Suzuki, K. Kobayashi, and S. Tanuma, Physica **105B**, 99 (1981).
- ²³ J. Qiao, X. Kong, Z.-X. Hu, F. Yang, and W. Ji, cond-mat/arXiv:1403.0499 (2014).
- ²⁴ Q. Wei and X. Peng, Appl. Phys. Lett **104**, 251915 (2014).
- ²⁵ J. Zhang, H. Liu, L. Cheng, J. Wei, J. Liang, D. Fan, J. Shi, X. Tang, and Q. J. Zhang, cond-mat/arXiv:1405.3348 (2014).
- ²⁶ H. Y. Lv, W. J. Lu, D. F. Shao, and Y. P. Sun, cond-mat/arXiv:1404.5171 (2014).
- ²⁷ K. Gong, L. Zhang, W. Ji, and H. Guo, cond-mat/arXiv:1404.7207 (2014).
- ²⁸ N. Rudenko and M. I. Katsnelson, Phys. Rev. B **89**, 201408 (2014).
- ²⁹ V. Tran and L. Yang, Phys. Rev. B **89**, 245407 (2014).
- ³⁰ K. Dolui, C. D. Pemmaraj, and S. Sanvito, ACS Nano **6**, 4823 (2012).
- ³¹ X. Peng, Q. Wei, and A. Copple, cond-mat/arxiv.org:1404.5995 (2014).
- ³² Y.-W. Son, M. L. Cohen, and S. G. Louie, Phys. Rev. Lett. **97**, 216803 (2006).
- ³³ X. Y. Zhao, C. M. Wei, L. Yang, and M. Y. Chou, Phys. Rev. Lett. **92**, 236805 (2004).
- ³⁴ L. Yang, C.-H. Park, Y.-W. Son, M. L. Cohen, and S. G. Louie, Phys. Rev. Lett. **99**, 186801 (2007).
- ³⁵ C.-H. Park and S. G. Louie, Nano Lett. **8**, 2200 (2008).
- ³⁶ L. S. Q Wu, M. Yang, Z. Huang, and Y. P. Feng, cond-mat/arxiv.org:1405.3077 (2014).
- ³⁷ V. Tran, R. Soklaski, Y. Liang, and L. Yang, Phys. Rev. B **89**, 235319 (2014).
- ³⁸ Z. Zhang and W. Guo, Phys. Rev. B **77**, 075403 (2008).
- ³⁹ X. N. Niu, D. Z. Yang, M. S. Si, and D. S. Xue, Applied Physics **115**, 143706 (2014).
- ⁴⁰ J. ÓKeefe, C. Y. Wei, and K. J. Cho, Appl. Phys. Lett. **80**, 676 (2002).
- ⁴¹ V. Barone and J. E. Peralta, Nano Letters **8**, 2210 (2008).
- ⁴² M. Ezawa, cond-mat/arxiv.org:1404.5788 (2014).
- ⁴³ S. Datta, *Electronic Transport in Mesoscopic Systems*. (Cambridge University Press, Cambridge, England, 1995).
- ⁴⁴ S. Datta, *Quantum Transport: Atom to Transistor*. (Cambridge University Press, Cambridge, England, 2005).